



Computer Programs in Physics

## GRANAD - Simulating GRAPhene nanoflakes with ADatoms

David Dams<sup>a,\*,</sup>, Miriam Kosik<sup>b</sup>, Marvin Müller<sup>a</sup>, Abhishek Ghosh<sup>b</sup>, Antton Babaze<sup>c,f,h</sup>, Julia Szczuczko<sup>b</sup>, Garnett W. Bryant<sup>c,d</sup>, Andrés Ayuela<sup>e,f</sup>, Carsten Rockstuhl<sup>a,g</sup>, Marta Pelc<sup>b</sup>, Karolina Słowik<sup>b</sup>

<sup>a</sup> Karlsruhe Institute of Technology, Institute of Theoretical Solid State Physics, Kaiserstr. 12, 76131 Karlsruhe, Germany<sup>b</sup> Institute of Physics, Nicolaus Copernicus University in Toruń, Grudziadzka 5/7, 87-100 Toruń, Poland<sup>c</sup> Joint Quantum Institute, University of Maryland and National Institute of Standards and Technology, College Park 20742, MD, USA<sup>d</sup> Nanoscale Device Characterization Division, National Institute of Standards and Technology, Gaithersburg 20899, MD, USA<sup>e</sup> Centro de Física de Materiales, CFM-MPC CSIC-UPV/EHU, Paseo Manuel Lardizabal 5, Donostia-San Sebastián 20018, Spain<sup>f</sup> Donostia International Physics Center (DIPC), Paseo Manuel Lardizabal 4, Donostia-San Sebastián 20018, Spain<sup>g</sup> Karlsruhe Institute of Technology, Institute of Nanotechnology, Kaiserstr. 12, 76131 Karlsruhe, Germany<sup>h</sup> Department of Applied Physics, School of Architecture, UPV/EHU, Donostia-San Sebastián 20018, Spain

## ARTICLE INFO

The review of this paper was arranged by Prof. Weigel Martin

## Keywords:

Graphene

Ssh chain

Nanoflakes

Adatoms

Dynamics

Tight binding

Simulations

Open source

## ABSTRACT

GRANAD is a program based on the tight-binding approximation to simulate optoelectronic properties of graphene nanoflakes and Su–Schrieffer–Heeger (SSH) chains with possible adatom defects under electromagnetic illumination. Its core feature is the numerical solution of a time-domain master equation for the spin-traced one-particle reduced density matrix. It provides time-resolved evolution of charge distributions, access to induced-field dynamics, and characterization of the plasmonic response. Other computable quantities include energy profiles, electron distribution in real space, and absorption spectra. GRANAD is written in Python and relies on the JAX library for high-performance array computing, just-in-time (JIT) compilation, and differentiability. It is intended to be lightweight, portable, and easy to set up, offering a transparent and efficient way to access the properties of low-dimensional carbon structures from the nanoscale to the mesoscopic regime. GRANAD is open source, with the full code and extensive documentation with usage examples available at <https://github.com/GRANADlauncher/granad.git>.

## Program summary

**Program Title:** GRANAD**CPC Library link to program files:** <https://doi.org/10.17632/723d4m4z9x.1>**Developer's repository link:** <https://github.com/GRANADlauncher/granad>**Licensing provisions:** MIT**Programming language:** Python**Supplementary material:** Code, documentation and demo files.

**Nature of problem:** Accessing the dynamical optical properties of graphene nanoflakes and one-dimensional polymer chains up to the mesoscale in the presence of adatoms represents a conceptual and computational challenge. Easily accessible classical methods fail as they do not accommodate relevant quantum effects. At the same time, quantum-mechanical *ab initio* time-domain approaches are computationally costly, and their implementations are often difficult for the user to set up and extend due to the high complexity of the codebase.

**Solution method:** A theoretical framework that combines an electronic mean-field approach with a Lindblad-like master equation is implemented to describe these carbon-based systems, where interaction with an external electric field is described semiclassically in the tight-binding approximation. Many-body effects are modeled via a nonlinear interaction term in the Hamiltonian, while dissipative processes are included in the master equation. Simulations are performed in the time domain, providing detailed access to physically relevant quantities. The implementation is lightweight, easily portable, and can be extended to incorporate other materials and nanoflake stacks.

\* Corresponding author.

E-mail address: [david.dams@kit.edu](mailto:david.dams@kit.edu) (D. Dams).<https://doi.org/10.1016/j.cpc.2025.109818>

Received 18 February 2025; Received in revised form 21 July 2025; Accepted 12 August 2025

Available online 26 August 2025

0010-4655/© 2025 The Author(s). Published by Elsevier B.V. This is an open access article under the CC BY license (<http://creativecommons.org/licenses/by/4.0/>).

*Additional comments including restrictions and unusual features:* The program relies on the JAX library, enabling differentiation of its core functions. It is intended to be extendable to, e.g., electric field parameter optimization for desired nanomaterial response and to popularize the differentiable programming technique further.

## 1. Introduction

Graphene is a two-dimensional carbon allotrope whose exotic properties have put it at the center of interest for various research communities [1–4]. Mesoscopic doped graphene flakes are a particularly promising optical platform [5] because their resonances typically fall in the near-infrared to visible range, enabling interactions with other optically active systems such as atoms or molecules [6]. Graphene is also highly tunable: Rapid progress in manufacturing and experimental techniques enables the fabrication of regular-shaped nanoflakes and perylene chains [7], as well as external control of doping, edge types [8], and defects. Their Fermi energy can be tailored by variation of external temperature, surrounding chemicals [9], and laser illumination [10]. This unlocks a wide variety of practical applications [8]. Another carbon-based material of high theoretical interest, especially for its topological [11] and nonlinear optical [12] properties, is the Su-Schrieffer-Heeger (SSH) chain, realized, e.g., in polyacetylene polymer chains [13].

The simulation of both graphene flakes and SSH chains up to the mesoscale and, particularly, their interaction with light presents a conceptual and computational challenge. For larger structures under long-wavelength external illumination, a classical description in terms of material parameters may be apt [14–16]. The response of mesoscopic flakes and polymer chains is determined by their atomistic arrangement, necessitating inherently more complex quantum mechanical approaches [5], requiring efficient implementations [17,18].

Recently, doping small graphene flakes with adatoms has come within experimental reach [19], offering a new potential platform to study phenomena at the interface of solid-state physics and quantum optics. Yet, modeling such structures is challenging as it requires bridging methodologies characteristic of the two realms to capture processes occurring at different size- and timescales within one coherent framework. The pioneering work on graphene nanoflakes of [5,20,21] has been extended to include adatoms in later works [22,6].

The challenge to model carbon structures up to the mesoscale in an easily interpretable yet efficient way prompts us to implement a hybrid method incorporating techniques from solid-state physics and the study of open quantum systems. To respond to such a challenge, we present *GR*aphene *N*anoflakes with *A*datoms (GRANAD), a lightweight and efficient open-source program for modeling the electronic and optical properties of graphene flakes as well as polyacetylene chains in the presence of adatoms. GRANAD is written in the Python programming language with the goal of being easily accessible and portable across various platforms. It exploits the JAX library for performance to contribute to its further popularization in scientific computing communities. To set up a simulation, GRANAD allows for a specification of the atomistic structure of a given material in a Lego-like fashion. The specification process is designed to be easy to use and mimics common object-oriented semantics. It operates mainly on Python primitives and is not performance-critical. The actual time propagation takes place by Just-in-time compilation (JIT compilation) of a composition of pure functions. This logical separation represents GRANAD’s user-friendly and efficient design principle.

The rest of this paper is structured as follows. In section 2, we introduce the theoretical framework behind GRANAD, centered around a time-domain master equation for the spin-traced one-particle reduced density matrix, from which physical properties can be computed. We then present the simulation program itself in section 3, and provide example results on optical characteristics of graphene nanoflakes and SSH chains in section 4. Comprehensive usage examples of GRANAD covering the steps of setup, actual simulation, and post-processing for a

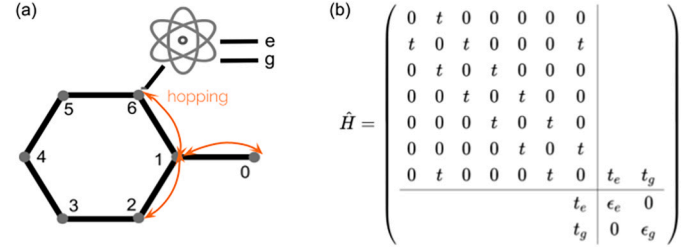


**Fig. 1.** (a) Example 7-site flake with a two-level adatom with the ground and excited states of energies  $\epsilon_g, \epsilon_e$  coupled to the 6th carbon site with the coupling strengths of  $t_g$  and  $t_e$ , respectively. The electron hopping between nearest-neighbor sites occurs with the rate  $t$ . (b) Hamiltonian of the given flake constructed following eq. (1). GRANAD can capture electron dynamics beyond the nearest-neighbor approximation both in the hopping energies and electron-electron interactions.

variety of physical problems and scenarios are available in the online manual. We discuss performance in 5, along with documentation and software management aspects of GRANAD in section 6, and conclude the paper in section 7.

## 2. Theoretical framework

The theoretical foundation of GRANAD is a Lindblad-like master equation utilizing a one-particle tight-binding approximation, introduced by J. Cox et al. [21] and extended in later works [6,23,24]. Along the same lines, GRANAD simulates the dynamics of the spin-traced one-particle reduced density matrix of  $p_z$  electrons in carbon structures. Henceforth, we refer to this quantity as the density matrix for short. The Hermitian part of the master equation incorporates both a semiclassical interaction with external electric fields and a nonlinear Coulomb interaction term. At the same time, dissipative processes are considered via a non-Hermitian relaxation term. Adatoms are modeled as multilevel systems electronically coupled to all or selected nanostructure sites. In the following, we summarize the theoretical framework.

### 2.1. Free Hamiltonian and density matrix

The one-particle tight-binding Hamiltonian reads as

$$H_{\text{tb}} = - \sum_{l,l'} t_{l,l'} (|l\rangle\langle l'| + |l'\rangle\langle l|) + \sum_{\alpha} t_{\alpha,\alpha} |\alpha\rangle\langle\alpha| - \sum_{l,\alpha} t_{l,\alpha} (|l\rangle\langle\alpha| + |\alpha\rangle\langle l|), \quad (1)$$

where the Latin index  $l$  numbers the carbon sites on the flake, and the Greek index  $\alpha$  labels adatom orbitals. We refer to the parameters  $t_{l,l'}$  as hopping energies set by default at  $t_{l,l'} = -2.66$  eV [25]. In general, they can be defined as functions of distance or the neighborhood index between the sites identified by  $l$  and  $l'$ . They are conceptualized as free parameters, sourced externally, e.g., from a Wannierization, fitting procedure or experiment. They can also be left entirely free in the case of explorative modeling. The diagonal term  $t_{l,l}$  is the  $l$ -th onsite energy. Similarly,  $t_{\alpha,\alpha}$  is the  $\alpha$ -th adatom orbital energy, while  $t_{l,\alpha}$  is the hopping rate between the  $l$ -th flake site and the  $\alpha$ -th adatom orbital. Extensive literature is devoted to details of modeling adatoms on graphene [26–29,6] where information of adatom energy levels and their coupling strengths with graphene can be found. Adatoms on graphene tend to localize in three possible positions: top - above a single graphene site, bridge - between a pair of sites, or hollow - in the middle of a selected hexagon. In general, fluorenes, hydroxyl groups, gold, silver adatoms

and carbon radicals favor top position and their coupling strengths tend to be comparable to the coupling among carbon sites on graphene. Non-metallic and a few metallic adatom types (Pd, Pt, Co) localize at the bridge position. Most of metallic adatoms including early transition metals prefer the hollow position, with couplings to six hexagon sites at least an order of magnitude weaker than the nearest-neighbor carbon-carbon coupling in graphene. For many applications, it is enough to consider a single adatom orbital to describe graphene nanostructures in the low energy range around the Fermi level [29].

A typical nanostructure, such as a basic 7-site flake is shown schematically in Fig. 1 with an adatom attached to site 6 with the couplings  $t_{6,e} = t_e$  and  $t_{6,g} = t_g$  between the 6th carbon site and the excited and ground states of the two-level adatom. The corresponding Hamiltonian matrix is shown. The Hamiltonian diagonalization provides the set of eigenstates  $|\varphi_j\rangle$  and the corresponding energies  $\epsilon_j$ . The eigenstates can be represented in the basis of discrete sites  $\{|L\rangle\}$  localized at positions of carbon atoms:  $|\varphi_j\rangle = \sum_L a_{jL}|L\rangle$ , where the index  $L \in \{l, \alpha\}$ , and the transition matrix with elements  $a_{jL}$  is unitary. Naturally, the set of eigenstates  $\{|\varphi_j\rangle\}$  also constitutes a basis. The two bases are convenient for complementary applications and are used in GRANAD.

### 2.1.1. Ground state density matrix

The ground state density matrix for an  $N$  electron system is constructed as a mixture of the lowest-energy one-particle eigenstates  $|\varphi_j\rangle$  according to the Aufbau principle [6]. We assume these eigenstates to be ordered by increasing energy and define a critical state index according to  $N_c = \lfloor \frac{N}{2} \rfloor$ . Denoting by  $N_< = \sum_{\epsilon < \epsilon_{N_c}}$  the number of eigenstates below the HOMO level and by  $N_ = \sum_{\epsilon = \epsilon_{N_c}}$  the number of degenerate eigenstates at the HOMO level, the ground state density matrix is diagonal in the energy basis

$$\rho = \sum_j \rho_{jj} |\varphi_j\rangle \langle \varphi_j|, \quad (2)$$

with

$$\rho_{jj} = \frac{1}{N} \begin{cases} 2 & \text{for } j < N_c, \\ \frac{N-2N_<}{N_ =} & \text{for } j = N_c, \\ 0 & \text{for } j > N_c, \end{cases} \quad (3)$$

where the factors of 2 originate from the fact that the density matrix is spin-traced, allowing for 2 electrons per eigenstate according to the Pauli principle, and  $\frac{1}{N}$  is a normalization factor such that  $\text{tr} \rho = 1$ . In the absence of degeneracy, eq. (2) reduces to the usual eigenbasis expression of the density matrix  $\rho = \frac{e^{-\beta H_{\text{tb}}}}{\text{tr} e^{-\beta H_{\text{tb}}}}$  at zero temperature ( $\beta \rightarrow \infty$ ). In the following, we refer to the ground state density matrix as the ground state for short. Note that the number of electrons  $N$  can, in general, differ from the number of carbon sites  $N_s$ . In this case, the system is doped with electrons ( $N > N_s$ ) or holes ( $N < N_s$ ), leading to a non-uniform charge distribution which induces Coulomb interactions in the ground state constructed according to eq. (2). In this case, the true ground state of the system has to be determined self-consistently such that the Coulomb repulsion vanishes.

### 2.1.2. Self-consistency

The  $N$ -electron ground-state in the presence of doping or adatoms corresponds to an inhomogeneous distribution of charge  $\rho_{LL}^{(n)}$ . Here,  $n$  is an iterative index. For the initial iteration,  $n = 0$ ,  $\rho^{(0)}$  is given by eq. (2). This distribution gives rise to the induced potential

$$\phi_{\text{ind}}^{(n)} = -eN \sum_{L,K} |L\rangle \langle L| v_{LK} \left( \rho_{KK}^{(n)} - \frac{1}{N_s} \right), \quad (4)$$

where  $v_{LK}$  is the Coulomb matrix describing the strength of interactions of electrons on sites  $L$  and  $K$ ,  $\frac{1}{N_s}$  represents a uniform distribution of charge and  $e$  is the elementary charge. The induced potential, added to the tight-binding Hamiltonian, modifies its eigenstates and

energies, based on which a new  $N$ -electron ground state  $\rho^{(n+1)}$  can be constructed analogously to eq. (2) based on new eigenstates  $|\varphi_j^{(n)}\rangle$ . The procedure is iteratively repeated until self-consistency is achieved, yielding a self-consistent Hamiltonian  $H_{\text{sc}}$  and density matrix  $\rho^{\text{sc}}$ . To smoothly converge the process, the Hamiltonian in subsequent iterations is constructed as

$$H^{(n+1)} = H^{(n)} - e(1 - p_{\text{mix}})\phi_{\text{ind}}^{(n-1)} - ep_{\text{mix}}\phi_{\text{ind}}^{(n)}, \quad (5)$$

where  $p_{\text{mix}} \in [0, 1]$  is set by default at  $p_{\text{mix}} = 0.05$  and can be reset by the user. For the initial iteration,  $H^{(0)} = H_{\text{tb}}$ .

## 2.2. Dynamics

Electromagnetic illumination drives electronic transitions in the system and gives rise to charge dynamics, which are tracked through a master equation, as described below.

### 2.2.1. Interaction with an electric field

GRANAD implements various types of external potentials, allowing for the exploration of different aspects of the optical response in the nanostructures under study.

Typical plane-wave excitation is modeled within the quasistatic coupling scheme, which gives rise to the external potential

$$\phi_{\text{ext}}(t) = - \left[ e \sum_L \mathbf{r}_L |L\rangle \langle L| + \mathbf{d}_{ge} |e\rangle \langle g| + \mathbf{d}_{ge} |g\rangle \langle e| \right] \cdot \mathbf{E}(t) \quad (6)$$

where  $\mathbf{E}(t)$  is a spatially uniform, time-dependent electric field,  $\mathbf{r}_L$  denotes the site positions in 3D space and  $\mathbf{d}_{ge} = e \langle g | \hat{\mathbf{r}} | e \rangle = \mathbf{d}_{eg}^*$  denotes the transition dipole moment (for illustration, we have focused on a single atomic transition). The first term in Eq. (6), diagonal in the site basis, accounts for the internal structure of the joint system of the flake and adatom. The two terms coupling the adatom states describe the transitions induced by the electric field in the adatom modeled as a point-like system. Currently, three types of electric fields are implemented: a continuous cosine-like illumination, a pulse characterized by a Gaussian envelope, and an initial kick perturbation represented by a Dirac delta, commonly used in linear-response calculations.

GRANAD also includes the implementation of an external potential generated by a point-like dipole emitter, which simulates the optical excitation of an atom or small molecule located near the nanostructure. This external potential is given by

$$\phi_{\text{ext}}^{\text{dip}}(\mathbf{r}, t) = \frac{1}{4\pi\epsilon_0} \mathbf{p}_{\text{dip}}(t) \cdot \frac{\mathbf{r} - \mathbf{r}_{\text{dip}}}{|\mathbf{r} - \mathbf{r}_{\text{dip}}|^3}, \quad (7)$$

where  $\mathbf{p}_{\text{dip}}(t)$  is the time-dependent dipole moment of the point-like emitter,  $\mathbf{r}_{\text{dip}}$  denotes its position and  $\epsilon_0$  the vacuum permittivity.

Additionally, GRANAD enables users to easily implement custom time- and spatially-dependent external potentials, such as the potential created by external, fast-electron beams or spatially modulated laser beams.

### 2.2.2. Coulomb Hamiltonian

The external field induces charge oscillations on the nanostructure. The redistributed charge gives rise to the time-dependent Coulomb potential

$$\phi_{\text{ind}}(t) = -eN_e \sum_{L,K} |L\rangle \langle L| v_{LK} (\rho_{KK}(t) - \rho_{KK}^{\text{sc}}), \quad (8)$$

where  $\rho(t)$  is the time-dependent density matrix of the system.

Both potentials are added to the Hamiltonian

$$H[\rho(t)] = H_{\text{sc}} + e\phi_{\text{ext}}(t) + e\phi_{\text{ind}}(t). \quad (9)$$

Note that the electron interactions  $v_{LK} \neq 0$  give rise to collective non-linear effects, e.g. in the plasmonic response [30,31]. Coulomb interactions, affecting the optical resonance positions of the system, play an

important role in the simulation of the nanostructure dynamics modifying, e.g., its absorption properties [22].

### 2.2.3. Master equation

A nonlinear master equation describes the dynamics of the electronic density matrix

$$\dot{\rho}(t) = -\frac{i}{\hbar} [H[\rho(t)], \rho(t)] + D[\rho(t)]. \quad (10)$$

Here,  $D[\rho(t)]$  is the relaxation functional discussed below.

### 2.2.4. Relaxation

GRANAD currently supports two relaxation models: phenomenological and Lindblad-equation based. The phenomenological model is used in literature to model relatively large ensembles of similar particles or atomic systems [32,33,21,30] and as such, is appropriate for relatively large nanostructures without adatoms. It describes the relaxation with a single parameter, the decoherence lifetime  $\tau$ :

$$D[\rho(t)] = -\frac{1}{2\tau} [\rho(t) - \rho^{\text{stat}}]. \quad (11)$$

Above,  $\rho^{\text{stat}}$  is a predefined stationary state to which the system relaxes, identified with the ground state of the system.

The recently introduced saturated Lindblad model [34] is more suitable for smaller nanostructures, especially those with adatoms. It allows one to capture different relaxation timescales related to, e.g., spontaneous emission in the hybridized adatom-nanostructure systems on the one hand, and electron-scattering- or phonon-induced dephasing in graphene on the other. In this model, the relaxation is described with the Lindblad term

$$D[\rho(t)] = \sum_k \gamma_k \left( L_k \rho(t) L_k^\dagger - \frac{1}{2} \{ L_k^\dagger L_k, \rho(t) \} \right), \quad (12)$$

where  $\gamma_k$  are relaxation rates for processes described by Lindblad operators  $L_k$ . To account for the Pauli principle in the one-electron approach, the  $\gamma_k$  are dynamically suppressed when the target state of the transition approaches full occupation [34].

All observable quantities are constructed from expectation values involving the trace of the density matrix. GRANAD focuses on the calculation of optical properties, such as induced charge distributions, dipole moments and electric fields, plasmonicity characterization *via* the energy-based plasmonicity index (EPI) [30], as well as energy and absorption spectra. A detailed list is given in the online documentation.

## 3. Program summary

In the following, we describe the operation of GRANAD. A simulation is organized into three steps: setup, solving the master equation and postprocessing. Setting up a simulation requires constructing a given finite structure as a list of orbitals. In this list, each orbital is represented by a dedicated object and can couple to any other orbital in a highly customizable way. Simulations are performed by mapping the orbitals and their couplings to arrays. These arrays are then processed by a function that is just-in-time-compiled to machine code for numerical integration of the master equation (10), based on the `diffraX` library [35]. The output of a simulation is an array of density matrices, sampled at user-specified points in time. From this array, time-dependent expectation values of any operator specified by the user can be computed and converted to the frequency domain with further built-in methods. Code examples are provided to accompany this formal description. In all these examples, we assume a preceding global import of both GRANAD and the JAX distribution of `numpy` as in Listing 1.

### 3.1. Main classes

GRANAD models orbitals, groups of orbitals and bulk materials with a corresponding class.

```
import granad
import jax.numpy as jnp
```

Listing 1: Global imports for the usage examples.

- An `Orbital` is a dataclass, analogous to a C struct containing optional fields specifying the position and a user-defined tag associated with the orbital. If unspecified, the orbital position defaults to the origin and the tag to `None`. There are no methods associated with this class.
- An `OrbitalList` is a collection of orbitals, offering insertion, deletion and addition operations like a regular Python list. It implements all numerical simulation methods and can be constructed in two ways: The user can define a custom orbital collection or it can be obtained as a finite cutout of an infinite material, as discussed next.
- A `Material` is characterized by an infinite lattice structure with additional information about orbital positions and couplings in the unit cell. Materials are exposed by a dedicated class, called `MaterialCatalog`. Currently, GRANAD supports two materials: `graphene` and `chain`, but the code is prepared for future extensions. Finite structures can be cut from the material instance by calling its `cut_flake` method. Currently supported shapes include triangular, hexagonal, diamond and rectangular geometries with armchair or zigzag type edges, as well as different types of SSH chains that may be used in particular to model polyacene or polyene structures. All these structures have been the subject of interest in numerous recent studies [36–38,30,6,23].

Listing 2 demonstrates the instantiation of two `OrbitalList`s to describe the following structures:

- A single adatom, modeled as a two-level system hosting a single electron. This system is created from two `Orbitals`, representing its ground and excited states with energies of  $\pm 0.5$  eV, which are combined into an `OrbitalList`.
- A triangular cut of the `Material` graphene, with a base length of 10 Å and an armchair edge type.

```
# adatom composed of ground and excited state orbitals
ground = granad.Orbital()
excited = granad.Orbital()
adatom = granad.OrbitalList([ground, excited])
adatom.set_onsite_hopping(ground, -0.5)
adatom.set_onsite_hopping(excited, 0.5)
adatom.set_electrons(1)

# cutting flake from Material
graphene = granad.MaterialCatalog.get("graphene")
flake = graphene.cut_flake(granad.Triangle(10, armchair = True))
```

Listing 2: Usage example - defining structures.

By default, GRANAD considers every orbital to contribute one electron to the structure. The structure is modeled as a closed-shell system, such that  $N$  electrons occupy the  $N/2$  lowest energy levels. This setting can be modified to account for electron or hole doping with the `set_electrons` function. The close analogy of `OrbitalList`s to regular Python lists can be exploited to define hybrid systems by list concatenation. Listing 3 demonstrates how to combine the previously defined flake and adatom by adding the adatom at the top position above the 16th carbon atom at a distance of 3Å. The resulting flake geometry and energy structure can then be visualized using built-in dedicated methods.

```
# creating hybrid system
coupling_site = flake[16]
adatom.set_position(coupling_site.position
+ jnp.array([3.0, 0, 0]))
flake_with_adatom = flake + adatom

# visualizing the final geometry and energy landscape
flake_with_adatom.show_2d(show_index=True)
flake_with_adatom.show_energies()
```

Listing 3: Plotting the structure and energy levels.

### 3.2. Coupling orbitals

The class `OrbitalList` offers dedicated functions to specify couplings, run simulations, and process results. Couplings are specified by the following private attributes of the `OrbitalList`:

1. The tight-binding Hamiltonian  $H_{\text{tb}}$  is represented by `_hamiltonian`.
2. The Coulomb interaction matrix  $v$  corresponds to `_coulomb`.
3. Dipole moment elements, e.g.,  $-e\mathbf{r}_{eg}$  for the adatom, are encoded by `_transitions`.

Each coupling is a hash table that is used to construct a matrix representation of the corresponding Hermitian operator. All couplings map a pair of orbitals to a value. For illustration, Listing 4 shows setting the following couplings: the transition dipole moment element in the adatom to 1 eÅ with an orientation along the  $x$  axis and hopping energies to 2.0 eV between the site of the flake to which the adatom is coupled and both adatom orbitals.

```
adatom.set_dipole_element(ground, excited, [1, 0, 0])
flake_with_adatom.set_hamiltonian_element(coupling_site,
adatom, 2.0)
```

Listing 4: Specifying the coupling.

Instead of coupling single orbitals, groups of orbitals can also be coupled. This is to facilitate, e.g., the coupling between the adatom and the graphene flake, potentially containing thousands of orbitals, where specifying each individual orbital combination is no longer feasible. The coupling does not need to have numerical values, but can also be an arbitrary function depending on the orbital distance. This allows a high degree of flexibility in configuring the tight-binding parameters during simulation setup and is covered extensively in the online documentation.

### 3.3. Running simulation and processing results

The `OrbitalList` exposes a method for running time-domain simulations. Listing 5 demonstrates such a simulation to compute the time-dependent single-particle energy occupations of the previously specified hybrid system where decoherence processes are captured via a decoherence time approximation according to (11) with a decoherence time of  $\hbar\tau^{-1} = 10$  meV. As discussed in [5], the exact value of this phenomenological parameter is expected to exert less influence on the resulting dynamics compared to finite size and edge effects, initial state with a single electron excited from the HOMO to the LUMO+2 level is considered. Coulomb interactions are turned off in this simulation by setting Coulomb interaction scaling parameter to 0. The actual simulation is performed by integrating the master equation (10) numerically when calling the method `master_equation`. This method returns an array of density matrices, the central quantity accessible from GRANAD. By default, the fifth-order Runge-Kutta method with adaptive step size is used. To reduce memory usage, instead of saving the full time-dependent

density matrix, one can specify a list of operators whose expectation values will be evaluated as an output. All additional optional arguments, including those to set alternative `diffraX`-based solvers and step size options are extensively documented online.

```
# setting the initial state
homo = flake_with_adatom.homo
lumo = flake_with_adatom.homo + 1
flake_with_adatom.set_excitation(homo, lumo + 2, 1)

# running the master equation
result=flake_with_adatom.master_equation(
relaxation_rate=0.1,
density_matrix=["occ_e"],
end_time=15,
coulomb_strength=0.
)
```

Listing 5: Running the simulation.

Listing 6 shows how to plot the structure, its energy levels and the results of the simulation performed in Listing 5. In Fig. 2(a), adatom sites with indices 18 and 19 overlap in space. In (b), the energy levels of the initial state are shown. Two adatom levels with energies  $\pm 0.5$  eV appear in between the HOMO and LUMO states of the flake; the electron, originally occupying the adatom ground state, is excited to the LUMO+2 state. The simulation results, shown in (c), present the time evolution of the states' occupancy in the energy basis.

```
flake_with_adatom.show_2d(show_index=True)
flake_with_adatom.show_energies()
flake_with_adatom.show_res(result)
```

Listing 6: Plotting the results.

To aid with common tasks in processing density matrices to compute physical quantities, such as the computation of expectation values, polarizabilities, or spectra, a variety of convenience methods exists, detailed in the extensive documentation. In the next section, we will demonstrate the versatility of this approach, considering specific examples.

It is also possible to consider optical relaxation channels captured by Wigner-Weisskopf transition rates accessible via a dedicated built-in function. These rates are defined as

$$\gamma_{ij} = \frac{\omega_{ij}^3 e^2}{3\pi\epsilon_0 \hbar c^3} \sum_{k=x,y,z} |\langle i|\mathbf{r}_k|j\rangle|^2. \quad (13)$$

Here,  $\hbar\omega_{ij}$  is the difference between single-particle energies  $E_i$  and  $E_j$ ,  $\langle i|\mathbf{r}|j\rangle$  is the matrix element of the position operator  $\mathbf{r}$  between states  $i$  and  $j$ ,  $\epsilon_0$  is the vacuum permittivity,  $\hbar$  is the reduced Planck constant, and  $c$  is the speed of light.

## 4. Usage examples

In this section, we illustrate the usage of GRANAD with four examples featuring the absorption spectra of linear SSH chains with adatoms, the plasmonicity of hexagonal graphene nanoflakes, charge dynamics on a triangular flake with a gold adatom, and the induced field distribution around a hexagonal-shaped flake, that reside at the lower end of the mesoscopic scale. Our fifth example addresses the real-time dynamics in a hybrid system composed of two nickel atoms and 8-acene, representative of a broader class of systems relevant to nanoscale electronic structure studies.

### Structure 1

Fig. 3a documents the absorption spectra obtained for a linear SSH chain of 70 sites with an adatom attached to site 35. The spectra are

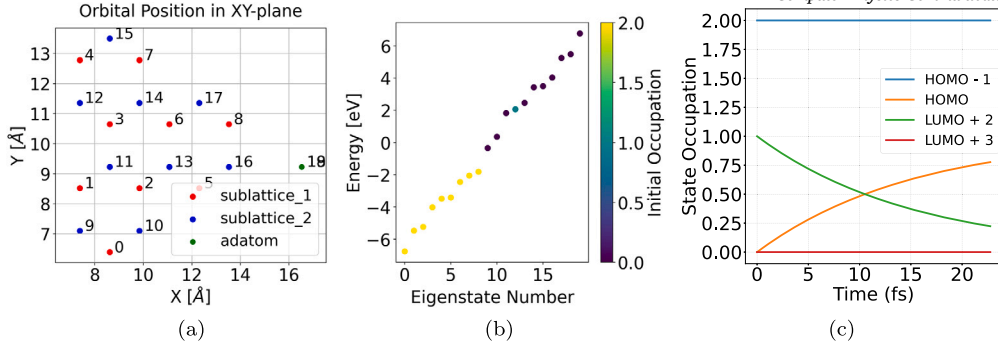


**Fig. 2.** (a) Structure of the flake + adatom hybrid system, the adatom sites with indices 18 and 19 overlapping in space; (b) the energy levels of the initial state. (c) simulation results - time evolution of the states' occupancy in the energy basis.

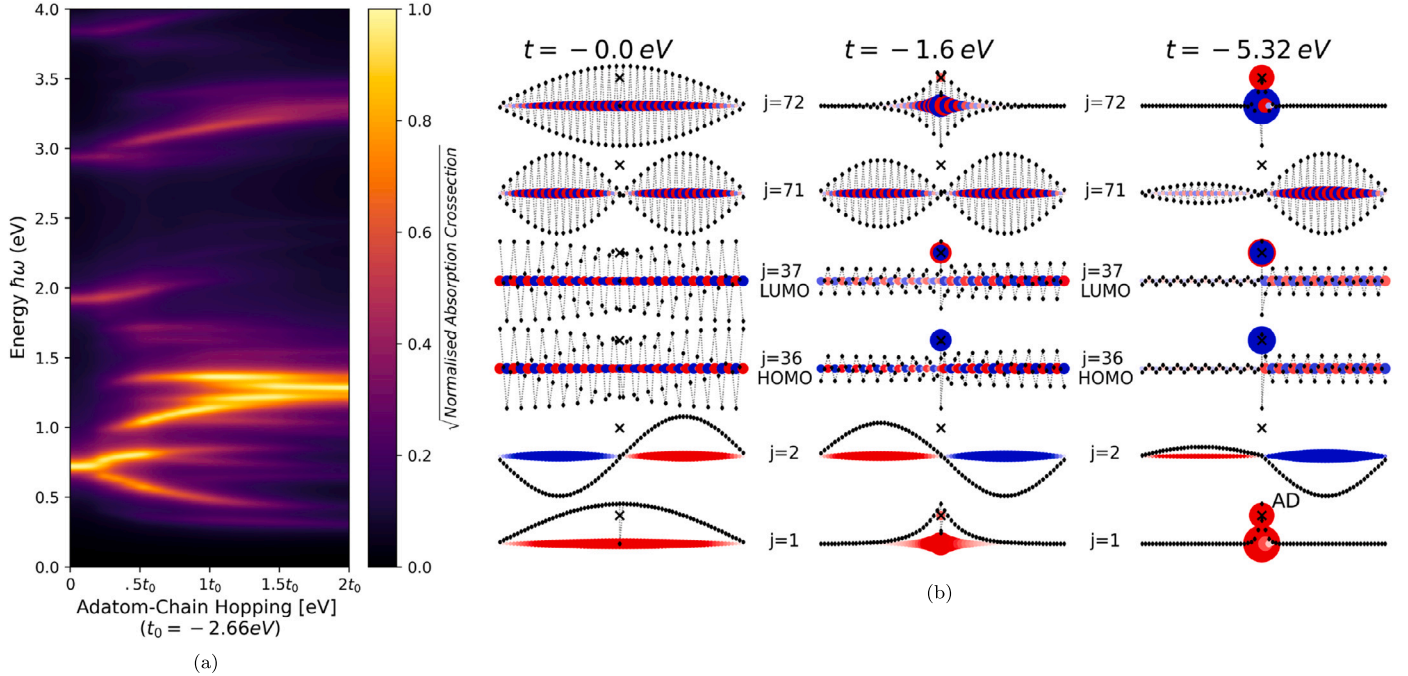


**Fig. 3.** (a) Square root of normalized absorption spectra for an undoped linear atomic chain with 70 sites and an adatom, for different adatom-chain coupling strength  $t = 0$  to  $2t_0$ , where  $t_0 = -2.66$  eV. (b) Real-space charge distribution (circles located at chain sites) of single-particle energy states for selected adatom-chain coupling strengths. The sizes and colors of the circles are proportional to  $|c_{ji}|^2$ . The distances of the diamonds above or below the sites of the chain represent values of the expansion coefficients at  $j^{\text{th}}$  site for the eigenstate  $|j\rangle$ , i.e.,  $c_{ji}$ .

shown as functions of the adatom-chain coupling strength  $t_{35,e} = t_{35,g} \equiv t$  and correspond to a decoupled chain-adatom system for  $t = 0$ . The energy of the main resonance approximately doubles as the adatom is strongly coupled near the middle of the chain, effectively splitting it into two sub-chains with eigenstates that tend to localize on the left- or right-hand side of the adatom as the coupling strength increases (Fig. 3b). The rich physics in the intermediate region leads to resonance splitting and avoided crossings. This system was analyzed in depth in Ref. [22].

**Structure 2** The energy-based plasmonicity index (EPI) has been developed as a measure of the collective character of optical resonances in nanoscaled molecular systems [30] ranging from 0 to 1. Fig. 4 shows the absorption spectrum of a 10 fold doped hexagonal nanoflake with the EPI values calculated for each absorption peak. The high EPI value of 0.62 associated with the resonance at 1.4 eV indicates the creation of an infrared plasmonic resonance due to doping, while other high energy peaks preserve their single-particle-like or mixed nature. The plasmonicity index of hexagonal and triangular nanoflakes was characterized in Refs. [30,31].

**Structure 3** The third example concerns the charge dynamics on a triangular graphene flake with a gold adatom. Based on Ref. [28], we

model the gold atom as a two-level system with its ground and excited states corresponding to the  $5d$  and  $6s$  orbitals, respectively with energies of  $-1.3$  eV and  $-0.3$  eV. In a free atom, the lower orbital is fully occupied and a single electron sits in the level close to the Fermi energy. We couple the adatom orbitals weakly to one of the corner sites  $l_c$  of the flake with  $t_e = t_g = -0.2 \times 2.66$  eV. Small changes of the coupling energies have weak impact on the overall optical response. The energies of the hybridized eigenstates and their initial occupation are shown in Fig. 5a. The charge distribution of the states that originate at the adatom, namely the highest occupied (HOMO) orbital and the orbital below (HOMO-1) is depicted in the inset of Fig. 5b. Due to optical selection rules, the transition dipole between the  $5d$  and  $6s$  adatom states vanishes. However, due to hybridization and charge transfer to the flake, a considerable dipole moment arises, as suggested by the charge distributions in the eigenstates and confirmed by calculations. As a result, upon a resonant continuous-wave illumination polarized along the  $x$  axis, the charge oscillates between the HOMO and HOMO-1 orbitals in cycles resembling Rabi oscillations (Fig. 5b). At times when the amplitude of these oscillations drops, other energy levels become active.

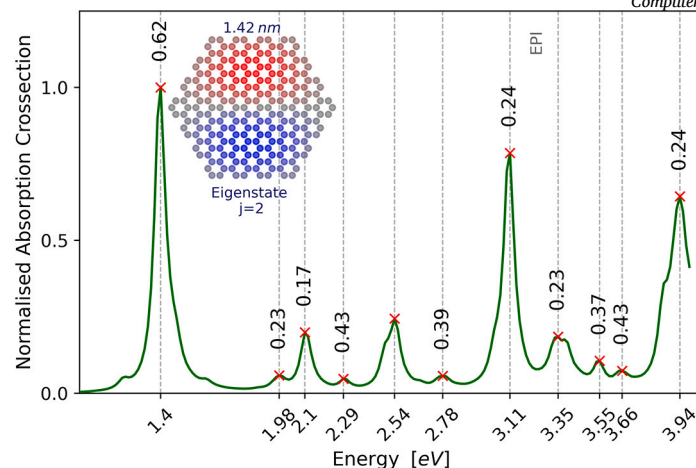


Fig. 4. Normalized absorption spectra and EPI corresponding to some of the transitions for a 10-fold doped hexagonal cut graphene nanoflake with each side having a length of 1.42 nm (4 hexagons/side). The inset shows the induced charge distribution in the first excited state of the flake.

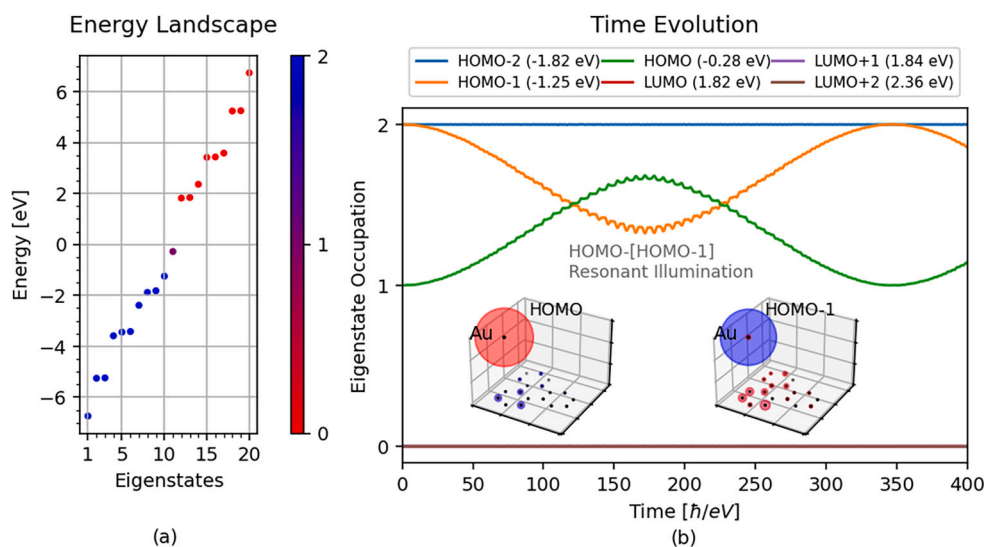


Fig. 5. (a) Eigenstates of an 10 fold doped, noninteracting triangular cut graphene nanoflake with an adatom coupled to a corner site of the flake in the plane. The color bar represents the ground state occupation of the eigenstates. (b) Time evolution of the HOMO and LUMO states of the system upon an  $x$ -polarized continuous resonant illumination of energy  $\hbar\omega = E_{\text{LUMO}} - E_{\text{HOMO}}$ . The adatom exhibits a transition dipole moment of 7.5 Debye, corresponding to approximately  $2.5 \times 10^{-29}$  Cm, along the  $x$ -direction. (For interpretation of the colors in the figure(s), the reader is referred to the web version of this article.)

Charge dynamics on graphene nanoflakes with adatoms was investigated in Ref. [6].

*Structure 4* Fig. 6 presents the induced-field distributions calculated with GRANAD around an armchair-edged hexagonal graphene flake with over 2500 carbon sites. The presented pattern for the field distribution is obtained for a continuous  $x$ -polarized plane-wave illumination at a resonant frequency  $\omega$  such that  $\hbar\omega = 0.66$  eV.

*Structure 5* Oligoacenes are a class of systems of prime importance for many technological applications, ranging from molecular devices to quantum computing [39,40]. They consist of linearly connected benzene rings with metal atoms attached. This hybrid system has opened up new paths in the functionalization of nanoscale materials [39]. Here, we consider a system composed of 8-acene, doped with two nickel atoms, placed at opposite ends of this quasi-1d structure at distances of 1 Å and 1.5 Å, respectively, from the 8-acene, illustrated in Fig. 7. We consider a single orbital per nickel and carbon atom, each contributing a single electron. We determine the geometric positioning of the nickel atoms following [39,41] and tight-binding parameters like in [42]. We adopt a distance-dependent form of the hopping  $t(r)$  between the nickel orbital and  $p_z$  carbon orbitals according to

$$t(r) = c \cdot \exp \left[ -q \left( \frac{r}{r_0} - 1 \right) \right], \quad (14)$$

where  $c = 0.261$  eV,  $q = 3.2$ ,  $r_0 = 1.8$  Å. Note that we have slightly adjusted the value for  $c$  compared to the  $p$ -orbital parameterization in Ref. [42] to achieve an energetic separation of 0.073 eV between the tight-binding eigenstates most localized on the nickel atoms. In analogy to the spin transfer results presented in [39], we focus on the transfer of electronic charge between the two nickel atoms. To this end, we illuminate the system with a Gaussian pulse centered around 40 fs, with a frequency of 0.07 eV, and a full width at half maximum of 56 fs. The results are displayed in Fig. 7.

Different types of dopants, such as transition metal atoms, can be taken into account similarly by adjusting the numerical parameters accordingly, as pointed out in [42] and following studies of TM-doped graphene [43,41]. This is the key strength of the parametric tight-binding approach employed by GRANAD. By trading accuracy for speed and scope, GRANAD positions itself as a versatile intermediary between highly accurate quantum and more phenomenological classical simulation frameworks.

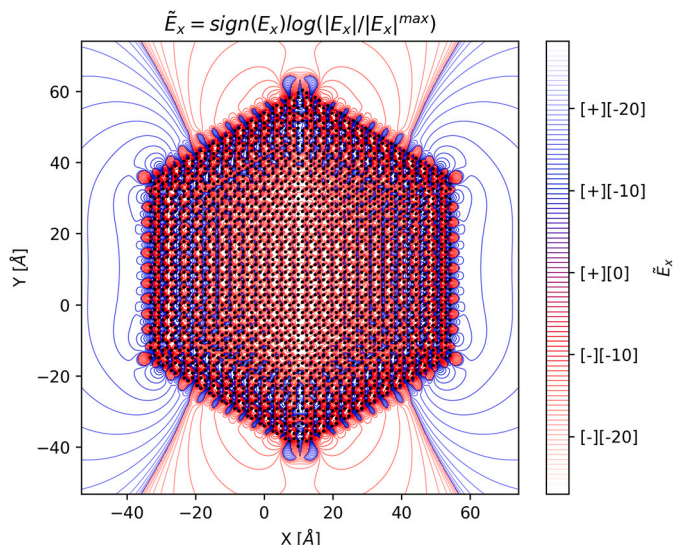


**Fig. 6.** Distribution of the  $x$ -component of the scattered electric field around an armchair-edged hexagonal flake made of 2520 carbon atoms subject to a resonant illumination. The electric field values are transformed using a logarithmic scale normalized to maximum field amplitude. The two square brackets in the color bar represent the phase and the scaled amplitude of the field respectively.

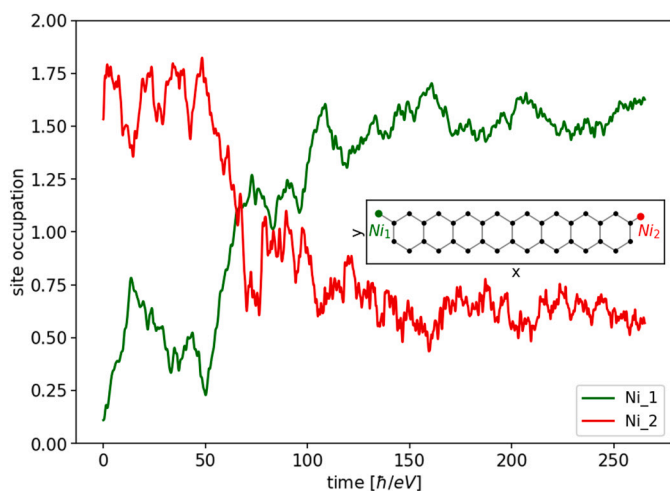


**Fig. 7.** Charge transfer dynamics in 8-acene doped with two nickel atoms. The hybrid system is considered under the illumination of a Gaussian pulse described in the main text, facilitating the transport of charge between the two nickel atoms located at opposite ends of the structure. The tight binding ground state at time  $t = 0$  suffers a slight reduction of the initial occupation of the two nickel atoms, corresponding to approximately 0.5 units of charge being contributed to the oligoacene. The inset displays the geometry of the system.

Scripts used to generate the results and Figs. 3-7 are available openly on the GRANAD GitHub repository. Please note there are many more example scripts available in the code documentation.

## 5. Code performance

Next, we analyze the performance of the GRANAD code, which is machine-specific. Fig. 8a presents the computation time required to simulate the optical response of systems containing between 270 and 13266 atoms. In these simulations, we consider triangular nanoflakes with armchair terminations, and the total simulation time is set to  $40 \hbar/eV$ . This duration ensures well-resolved excitation features in the frequency domain after applying a time-to-frequency Fourier transform. The resulting absorption spectra are shown in Fig. 9.

For benchmarking, we utilized the Hyperion supercomputer at the Donostia International Physics Center (DIPC). Hyperion consists of 232 nodes with a total of 12336 cores. Most nodes are equipped with either Intel Xeon Gold 6248R (Cascadelake) or Intel Xeon Gold 6342 (Icelake) processors. In our benchmark calculations, we used 24 cores on a single node, represented by the red points in Fig. 8a. The solid red line shows a fit to the data, following the relationship  $t \propto N^a$ , where  $a = 2.9$ . This power-law dependence aligns with the computational complexity of the algorithm, where direct integration of Eq. (10) involves matrix multiplications that scale as  $\mathcal{O}(N^3)$ . Additional benchmarks conducted on the ATLAS supercomputer, with varying numbers of cores, are also shown in Fig. 8a. These results exhibit a similar scaling, further validating the observed performance trends.

Moreover, the performance of GRANAD can be significantly enhanced when deployed on Graphics Processing Units (GPUs). As illustrated in Fig. 8b, the computation time for addressing the electron dynamics of triangular nanoflakes is drastically reduced when using an NVIDIA A100 PCIe GPU, compared to using e.g. an Intel Xeon Platinum 8358.

## 6. Documentation and software management

GRANAD is extensively documented using Sphinx. The software and its documentation, including a complete description of all public datatypes and functions as well as usage examples and setup installations, are hosted on GitHub, which also provides continuous integration. GRANAD is fully open-sourced under the MIT license. Installation of the newest version can take place via the pip command

```
pip install git+https://github.com/GRANADlauncher/granad.git
```

provided both git and Python pip are installed. A complete list of the packages GRANAD depends on is given in the pyproject.toml in the official GitHub repository. The newest official documentation is available at <https://granadlauncher.github.io/granad/>.

## 7. Conclusion

We have presented GRANAD, a simulation program to investigate the optoelectronic properties of systems composed of carbon-based low-dimensional nanostructures with adatoms in a tight-binding framework. Its main capability is the numerical integration of a time-domain master equation for the spin-traced one-particle reduced density matrix, taking into account many-body as well as dissipative effects. GRANAD offers access to static as well as dynamic quantities and includes the possibility of studying the time evolution of initially excited states. A semiclassical approximation allows us to take into account the influence of time-harmonic, potentially pulsed, or ramped-up electric fields. The theoretical approach taken by GRANAD allows us to simulate the interplay between charge dynamics, external electric fields, and dissipative effects in a carbon-based nanomaterial of finite extent to high detail. GRANAD is intended to expedite the computation of optical properties of nanomaterials in structures of up to mesoscopic scales, as its implementation is lightweight and designed to be easily usable. Planned future extensions include the capability to model multiple orbitals in layered 2D structures, microscopic electromagnetic field effects at the level of the Peierls substitution [44] as well as to exploit the differentiable capabilities offered by JAX in parametric investigations of nanomaterial properties.

## CRediT authorship contribution statement

**David Dams:** Conceptualization, Software. **Miriam Kosik:** Software. **Marvin Müller:** Software. **Abhishek Ghosh:** Software. **Antton Babaze:**

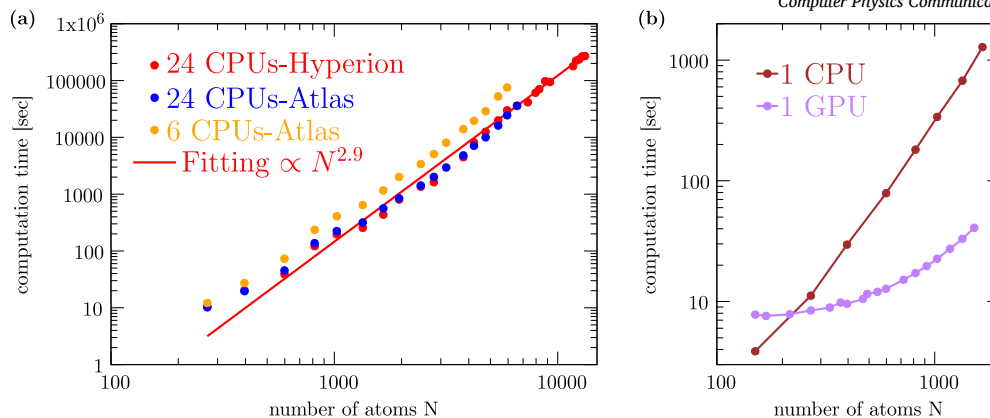


**Fig. 8.** (a) Computation time as a function of the number of atoms  $N$  for simulating the time evolution of triangular nanoflakes with armchair termination. The dashed-dotted red line represents a fitting function of the form  $N^a$ , where  $a = 2.9$ . The simulations have been run using different number of CPUs of either the supercomputer Hyperion or Atlas. See the labels for specific details. The total simulated time is  $40 \hbar/eV$ . (b) The code has been executed using a single Intel Xeon Platinum 8358 on Hyperion (brown line) or a NVIDIA A100 PCIe GPU (purple line). The total simulated time is  $4 \hbar/eV$ .

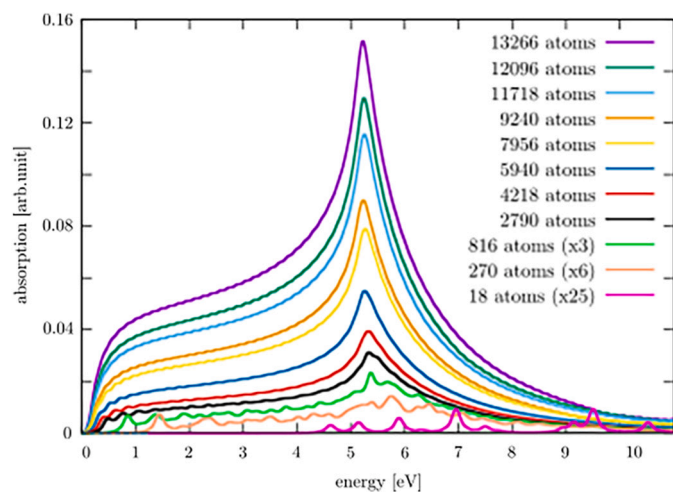


**Fig. 9.** Absorption spectra of undoped triangular nanoflakes with armchair termination for different numbers of atoms  $N$ . A hopping parameter of  $2.66 \text{ eV}$  and a propagation time of  $40 \hbar/eV$  are used.

Software. **Julia Szczuczko:** Software. **Garnett W. Bryant:** Conceptualization. **Andrés Ayuela:** Conceptualization. **Carsten Rockstuhl:** Conceptualization. **Marta Pelc:** Conceptualization. **Karolina Słowik:** Conceptualization.

#### Declaration of competing interest

The authors declare that they have no known competing financial interests or personal relationships that could have appeared to influence the work reported in this paper.

#### Acknowledgements

D.D. and C.R. acknowledge support by the German Research Foundation within the Project (RO 3640/14-1 under project number - 465163297). M.M.M. and C.R. acknowledge support by the German Research Foundation within the Project (RO 3640/8-1 under project number 378579271). A.G., M.P., and K.S. acknowledge support from the National Science Centre, Poland (Project No. 2020/39/I/ST3/00526) and are grateful to the Donostia International Physics Center for their kind hospitality. A.A. and A.B. acknowledge funding from the Spanish Ministry of Science and Innovation (grants nos. PID2022-139230NB-I00, and TED2021-132074B-C32), the Gobierno Vasco UPV/EHU (project no. IT-1569-22), the European Commission MIRACLE project (GA

964450), and NaturSea-PV (GA 101084348); research conducted in the scope of the Transnational Common Laboratory (LTC) Aquitaine-Euskadi Network in Green Concrete and Cement-based Materials.

Mention of commercial products is done to provide a complete description of the work done. The mention does not mean an endorsement or validation by NIST.

#### Data availability

No data was used for the research described in the article.

#### References

- [1] J.M. Link, P.P. Orth, D.E. Sheehy, J. Schmalian, Universal collisionless transport of graphene, *Phys. Rev. B* 93 (2016), <https://doi.org/10.1103/physrevb.93.235447>.
- [2] Y. Wu, D.B. Farmer, F. Xia, P. Avouris, Graphene electronics: materials, devices, and circuits, *Proc. IEEE* 101 (7) (2013) 1620–1637, <https://doi.org/10.1109/JPROC.2013.2260311>.
- [3] Y. Fan, N.-H. Shen, F. Zhang, Q. Zhao, H. Wu, Q. Fu, Z. Wei, H. Li, C.M. Soukoulis, Graphene plasmonics: a platform for 2d optics, *Adv. Opt. Mater.* 7 (3) (2019) 1800537, <https://doi.org/10.1002/adom.201800537>, <https://onlinelibrary.wiley.com/doi/pdf/10.1002/adom.201800537>.
- [4] A.K. Geim, Graphene: status and prospects, *Science* 324 (5934) (2009) 1530–1534, <https://doi.org/10.1126/science.1158877>, <https://www.science.org/doi/pdf/10.1126/science.1158877>.
- [5] S. Thongrattanasiri, A. Manjavacas, F.J. García de Abajo, Quantum finite-size effects in graphene plasmons, *ACS Nano* 6 (2) (2012) 1766–1775, <https://doi.org/10.1021/nl204780e>.
- [6] M. Kosik, M.M. Müller, K. Słowik, G. Bryant, A. Ayuela, C. Rockstuhl, M. Pelc, Revising quantum optical phenomena in adatoms coupled to graphene nanoantennas, *J. Nanophotonics* 11 (14) (2022) 3281–3298, <https://doi.org/10.1515/nanoph-2022-0154>.
- [7] K. Müllen, Evolution of graphene molecules: structural and functional complexity as driving forces behind nanoscience, *ACS Nano* 8 (7) (2014) 6531–6541, <https://doi.org/10.1021/nl503283d>.
- [8] V. Kumar, Linear and nonlinear optical properties of graphene: a review, *J. Electron. Mater.* 50 (7) (2021) 3773–3799, <https://doi.org/10.1007/s11664-021-08904-w>.
- [9] J. Yuan, L.-P. Ma, S. Pei, J. Du, Y. Su, W. Ren, H.-M. Cheng, Tuning the electrical and optical properties of graphene by ozone treatment for patterning monolithic transparent electrodes, *ACS Nano* 7 (5) (2013) 4233–4241, <https://doi.org/10.1021/nl400682u>.
- [10] H.L. Calvo, H.M. Pastawski, S. Roche, L.E.F.F. Torres, Tuning laser-induced band gaps in graphene, *Appl. Phys. Lett.* 98 (23) (2011) 232103, <https://doi.org/10.1063/1.3597412>, [https://pubs.aip.org/aip/apl/article-pdf/doi/10.1063/1.3597412/14451667/232103\\_1\\_online.pdf](https://pubs.aip.org/aip/apl/article-pdf/doi/10.1063/1.3597412/14451667/232103_1_online.pdf).
- [11] A.M. Marques, R.G. Dias, Multihole edge states in Su-Schrieffer-Heeger chains with interactions, *Phys. Rev. B* 95 (2017) 115443, <https://doi.org/10.1103/PhysRevB.95.115443>.
- [12] C. Jürß, D. Bauer, High-harmonic generation in Su-Schrieffer-Heeger chains, *Phys. Rev. B* 99 (2019) 195428, <https://doi.org/10.1103/PhysRevB.99.195428>.
- [13] A. Sivan, M. Orenstein, Topology of multiple cross-linked Su-Schrieffer-Heeger chains, *Phys. Rev. A* 106 (2022) 022216, <https://doi.org/10.1103/PhysRevA.106.022216>.

- [14] M. Jablan, H. Buljan, M. Soljačić, Plasmonics in graphene at infrared frequencies, *Phys. Rev. B* 80 (2009) 245435, <https://doi.org/10.1103/PhysRevB.80.245435>.
- [15] A. Ferreira, J. Viana-Gomes, J. Nilsson, E.R. Mucciolo, N.M.R. Peres, A.H. Castro Neto, Unified description of the dc conductivity of monolayer and bilayer graphene at finite densities based on resonant scatterers, *Phys. Rev. B* 83 (2011) 165402, <https://doi.org/10.1103/PhysRevB.83.165402>.
- [16] A. Kuc, T. Heine, G. Seifert, Structural and electronic properties of graphene nanoflakes, *Phys. Rev. B* 81 (2010) 085430, <https://doi.org/10.1103/PhysRevB.81.085430>.
- [17] P. Cosme, J.S. Santos, J.P. Bizarro, I. Figueiredo, Tethys: a simulation tool for graphene hydrodynamic models, *Comput. Phys. Commun.* 282 (2023) 108550, <https://doi.org/10.1016/j.cpc.2022.108550>.
- [18] P. Sony, A. Shukla, A general purpose Fortran 90 electronic structure program for conjugated systems using Pariser–Parr–Pople model, *Comput. Phys. Commun.* 181 (4) (2010) 821–830, <https://doi.org/10.1016/j.cpc.2009.12.015>.
- [19] M. Kaur, M. Kaur, V.K. Sharma, Nitrogen-doped graphene and graphene quantum dots: a review on synthesis and applications in energy, sensors and environment, *Adv. Colloid Interface Sci.* 259 (2018) 44–64.
- [20] A. Manjavacas, S. Thongrattanasiri, F.J.G. de Abajo, Plasmons driven by single electrons in graphene nanoislands, *J. Nanophotonics* 2 (2) (2013) 139–151.
- [21] J.D. Cox, F. Javier García de Abajo, Electrically tunable nonlinear plasmonics in graphene nanoislands, *Nat. Commun.* 5 (1) (2014) 5725, <https://doi.org/10.1038/ncomms6725>.
- [22] M.M. Müller, M. Kosik, M. Pelc, G.W. Bryant, A. Ayuela, C. Rockstuhl, K. Slowik, Modification of the optical properties of molecular chains upon coupling to adatoms, *Phys. Rev. B* 104 (23) (2021) 235414, <https://doi.org/10.1103/PhysRevB.104.235414>.
- [23] F. Aguilón, A.G. Borisov, Atomic-scale defects might determine the second harmonic generation from plasmonic graphene nanostructures, *J. Phys. Chem. Lett.* 14 (1) (2023) 238–244, <https://doi.org/10.1021/acs.jpcclett.2c03205>.
- [24] M. Pelc, D. Dams, A. Ghosh, M. Kosik, M.M. Müller, G.W. Bryant, C. Rockstuhl, A. Ayuela, K. Slowik, Single-particle approach to many-body relaxation dynamics, *Phys. Rev. A* 109 (2) (2024) 022237, <https://doi.org/10.1103/PhysRevA.109.022237>.
- [25] D. Tománek, S.G. Louie, First-principles calculation of highly asymmetric structure in scanning-tunneling-microscopy images of graphite, *Phys. Rev. B* 37 (1988) 8327–8336, <https://doi.org/10.1103/PhysRevB.37.8327>, <https://link.aps.org/doi/10.1103/PhysRevB.37.8327>.
- [26] K. Nakada, A. Ishii, Dft calculation for adatom adsorption on graphene, in: *Graphene Simulation*, 2011, pp. 1–19.
- [27] S. Ihnatsenka, G. Kirczenow, Dirac point resonances due to atoms and molecules adsorbed on graphene and transport gaps and conductance quantization in graphene nanoribbons with covalently bonded adsorbates, *Phys. Rev. B, Condens. Matter Mater. Phys.* 83 (24) (2011) 245442.
- [28] M. Amft, B. Sanyal, O. Eriksson, N.V. Skorodumova, Small gold clusters on graphene, their mobility and clustering: a dft study, *J. Phys. Condens. Matter* 23 (20) (2011) 205301.
- [29] E.J. Santos, A. Ayuela, D. Sánchez-Portal, Universal magnetic properties of sp<sup>3</sup>-type defects in covalently functionalized graphene, *New J. Phys.* 14 (4) (2012) 043022.
- [30] M.M. Müller, M. Kosik, M. Pelc, G.W. Bryant, A. Ayuela, C. Rockstuhl, K. Slowik, Energy-based plasmonicity index to characterize optical resonances in nanostructures, *J. Phys. Chem. C* 124 (44) (2020) 24331–24343, <https://doi.org/10.1021/acs.jpcc.0c07964>.
- [31] M.M. Müller, M. Kosik, M. Pelc, G.W. Bryant, A. Ayuela, C. Rockstuhl, K. Slowik, From single-particle-like to interaction-mediated plasmonic resonances in graphene nanoantennas, *J. Appl. Phys.* 129 (9) (2021), <https://doi.org/10.1063/5.0038883>.
- [32] H. Wang, J.H. Strait, P.A. George, S. Shivaraman, V.B. Shields, M. Chandrashekar, J. Hwang, F. Rana, M.G. Spencer, C.S. Ruiz-Vargas, et al., Ultrafast relaxation dynamics of hot optical phonons in graphene, *Appl. Phys. Lett.* 96 (8) (2010).
- [33] M. Breusing, S. Kuehn, T. Winzer, E. Malić, F. Milde, N. Severin, J. Rabe, C. Ropers, A. Knorr, T. Elsaesser, Ultrafast nonequilibrium carrier dynamics in a single graphene layer, *Phys. Rev. B, Condens. Matter Mater. Phys.* 83 (15) (2011) 153410.
- [34] M. Pelc, D. Dams, A. Ghosh, M. Kosik, M.M. Müller, G. Bryant, C. Rockstuhl, A. Ayuela, K. Slowik, Single-particle approach to many-body relaxation dynamics, *Phys. Rev. A* 109 (2) (2024) 022237.
- [35] P. Kidger, On Neural Differential Equations, Ph.D. thesis, University of Oxford, 2021.
- [36] P. Sony, A. Shukla, Large-scale correlated calculations of linear optical absorption and low-lying excited states of polyacenes: pariser-parr-pople Hamiltonian, *Phys. Rev. B, Condens. Matter Mater. Phys.* 75 (15) (2007) 155208.
- [37] T. Basak, H. Chakraborty, A. Shukla, Theory of linear optical absorption in diamond-shaped graphene quantum dots, *Phys. Rev. B* 92 (20) (2015) 205404.
- [38] D.K. Rai, A. Shukla, Excited states and optical properties of hydrogen-passivated rectangular graphenes: a computational study, *Sci. Rep.* 9 (1) (2019) 7958.
- [39] X. Liang, S. Ma, B. Ma, Y. Zhang, J. Liu, C. Li, G. Lefkidis, W. Hübner, W. Jin, Ultrafast spin transfer and spin logic gates in linear ni substituted polyacene structures, *Phys. Rev. B* 109 (2024) 064419, <https://doi.org/10.1103/PhysRevB.109.064419>, <https://link.aps.org/doi/10.1103/PhysRevB.109.064419>.
- [40] J.-i. Aihara, H. Kanno, Local aromaticities in large polyacene molecules, *J. Phys. Chem. A* 109 (16) (2005) 3717–3721, PMID: 16839039.
- [41] E.J. Santos, A. Ayuela, D. Sánchez-Portal, First-principles study of substitutional metal impurities in graphene: structural, electronic and magnetic properties, *New J. Phys.* 12 (5) (2010) 053012.
- [42] H. Amara, J.-M. Roussel, C. Bichara, J.-P. Gaspard, F. Ducastelle, Tight-binding potential for atomistic simulations of carbon interacting with transition metals: application to the Ni-C system, *Phys. Rev. B* 79 (2009) 014109, <https://doi.org/10.1103/PhysRevB.79.014109>, <https://link.aps.org/doi/10.1103/PhysRevB.79.014109>.
- [43] E.J. Santos, D. Sánchez-Portal, A. Ayuela, Magnetism of substitutional co impurities in graphene: realization of single  $\pi$  vacancies, *Phys. Rev. B, Condens. Matter Mater. Phys.* 81 (12) (2010) 125433.
- [44] J. Li, D. Golez, G. Mazza, A.J. Millis, A. Georges, M. Eckstein, Electromagnetic coupling in tight-binding models for strongly correlated light and matter, *Phys. Rev. B* 101 (5) (2020), <https://doi.org/10.1103/physrevb.101.205140>.